Nonlinear Dyn (2007) 50:587–596
DOI 10.1007/s11071-006-9178-x

ORIGINAL ARTICLE

Experimental study of an impact oscillator with viscoelastic and Hertzian contact

B. P. Mann · R. E. Carter · S. S. Hazra

Received: 1 May 2006 / Accepted: 6 July 2006 / Published online: 26 January 2007

Abstract Modeling an impact event is often related to the desired outcome of an impact oscillator study. If the only intent is to study the dynamic behavior of the system, numerous researchers have shown that simpler impact models will often suffice. However, when the geometric contours and material properties of the two colliding surfaces are known, it is often of interest to model the contact event at a greater level of complexity. This paper investigates the application of a finite time impact model to the study of a parametrically excited planar pendulum subjected to a motion-dependent discontinuity. Experimental and numerical studies demonstrate the presence of multiple periodic attractors, subharmonics, quasi-periodic motions, and chaotic oscillations.

Keywords Impact oscillator · Hertzian contact · Viscoelastic impact · Chaotic oscillations

1 Introduction

The behavior of piecewise smooth dynamical systems has practical relevance to many areas of science and engineering. For instance, motion-dependent discontinuities are often deliberately included in machinery designs to accommodate part tolerances, a working clearance, or the finite accuracy of a manufacturing process [1, 2]. Other examples include gear trains with backlash, systems with dry friction, and the application of impact dampers for vibration amplitude reduction. Much of the previous work on impacting systems has focused on piecewise linear systems that have a discontinuity in the force–displacement relationship. Although these systems are piecewise linear, the mere presence of a discontinuity – in these otherwise linear systems – allows for the manifestation of highly nonlinear behavior [3].

This paper examines the dynamic behavior of a parametrically excited planar pendulum that encounters a barrier at the downward position – a mechanical system with an archetypal motion-dependent discontinuity (see Fig. 1). Studying the oscillatory behavior of this system requires a proper model for the contact event. The first level of modeling complexity considers a constant coefficient of restitution, which is often estimated from empirical velocity data that may be implemented to capture the response behavior associated with a hard impact [4]. Alternatively, some researchers have suggested the implementation of a velocity-dependent coefficient of restitution or even modeling the impact event with an impulsive force [5, 6]. However, a conceptual problem exists for both alternatives since the impact time duration is assumed to be instantaneous.

B. P. Mann (✉) · S. S. Hazra
Dynamical Systems Laboratory, Department of Mechanical and Aerospace Engineering, University of Missouri, E3412 Lafferre Hall, Columbia, MO 65211, USA
e-mail: mannbr@missouri.edu

R. E. Carter
Engineer, USAF, Eglin AFB, FL 32611, USA

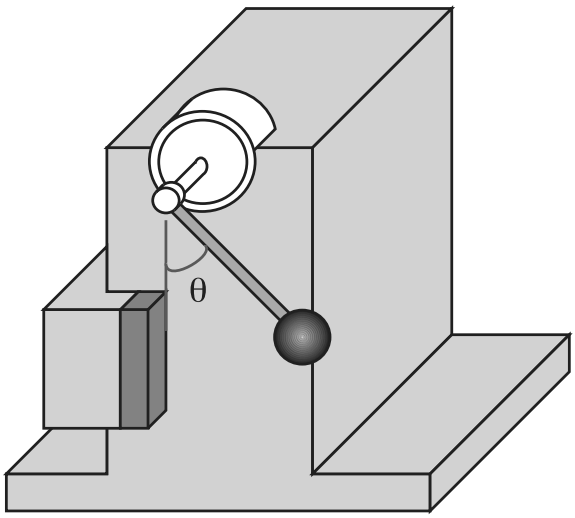

Fig. 1 Schematic diagram of the experimental pendulum fixture, the potentiometer, and the polymer impact barrier (shown in *black*). The above angular position is taken to be negative with positive angles assumed to occur when the sphere is in contact with the barrier

Modeling the impact as a finite time event is one alternative to a coefficient of restitution approach. The first level of complexity considers soft impact with linear force–deformation and force–velocity relationships. This type of model has been widely implemented to study piecewise linear oscillators, e.g., see references [7, 8], and provides a more realistic physical representation of an impact by including both a nonzero contact time and a contact force that is motion and/or velocity dependent [9]. In spite of these advantages, the typical Kelvin–Voigt model does not correspond to the realistic behavior encountered at the beginning and end of impact [10, 11].

The next level of complexity considers conformal contact of finite time duration where nonlinear force–deformation and/or force–velocity relationships are implemented. One of the the most prolific examples is that of Hertzian contact between a rigid sphere and an elastic half-space [12, 13]. The focus of this manuscript is to study the dynamic behavior of a parametrically excited pendulum with finite time impact events that are modeled by Hertz's contact law for elastic conformal contact along with a nonlinear force–velocity relationship [10, 11]. Although nonlinear, these relationships have the potential advantage of replicating the realistic force relationships at the beginning and end of impact. It is believed that the current work complements the previous studies of references [4, 6, 14] who treat the impact event as an instantaneous event, either by the application of a coefficient of restitution or through the incorporation of an impulse force.

The present work is organized as follows. The next section describes the experimental impact oscillator and the primary instrumentation used during the experimental study. The third section describes a model for the parametrically excited pendulum and the impact event. System identification of the experimental nonlinear system is separated into contact and noncontact regimes. Approximate analytical solutions are applied for the noncontact oscillations and numerical efforts are applied to match the experimental behavior with the observed impact oscillations. Experimental results and numerical comparisons are then presented to study the forced oscillations of a system that exhibits periodic, subharmonic, quasi-periodic, and chaotic behavior.

2 Description of experimental apparatus

A schematic diagram of the experimental impact oscillator of interest is shown in Fig. 1. Measurements of the pendulum's angular oscillations were obtained by supplying a constant voltage to a Novatechnik,[1] model P2200, low-torque potentiometer and recording the time varying voltage provided by the potentiometer's change in internal resistance. A unique feature of this potentiometer is the internal conductive plastic track, which provides a uniformly scaled analog voltage. This feature differs from the typical wire-wound potentiometer that results in step voltage changes.

The potentiometer was housed in a rigid base fixture and connected to a stainless steel, $l = 50$ mm long, threaded rod that was inserted into a 19 mm diameter stainless steel sphere. The total mass of assembled pendulum was measured to be $m = 32.6$ g. The pendulum base fixture was machined from aluminum 7050-T6 and mounted onto an air bearing shake table that was connected to an APS Dynamics, model 113, shaker (see Fig. 2). During the forced oscillation experiments, the motion of the shake table was measured with a Micro-Epsilon, model LD-1605-100, analog laser displacement sensor. To aid in the construction of experimental Poincaré sections, a Terahertz

[1] Commercial equipment is identified for completeness and does not necessarily imply endorsement by the authors.

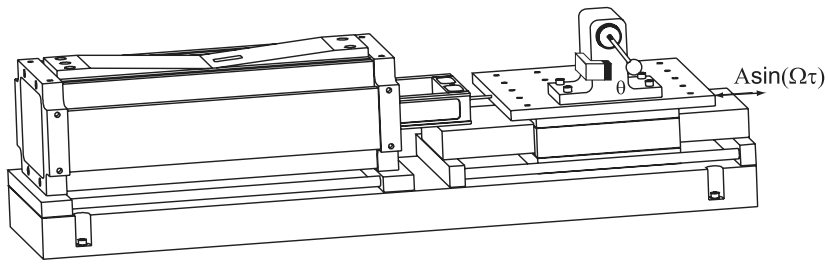

Fig. 2 Diagram of the electromagnetic shaker and experimental fixture that was fastened to the air bearing shake table

Technologies, model LT-850, laser tachometer was used to provide a once per period timing signal.

3 Impacting pendulum model

This section derives the governing equations for a horizontally shaken pendulum that encounters a barrier when the pendulum angular position is $\theta > 0$ (see Fig. 1). The impact condition is modeled as a finite time process where a rigid sphere penetrates a viscoelastic material. The kinetic energy for the pendulum, horizontally shaken at an excitation frequency of Ω, is

$$T = \frac{1}{2}m[(A\Omega\ \cos\Omega t - L\dot{\theta}\ \cos\theta)^2 + (L\dot{\theta}\ \sin\theta)^2] \tag{1}$$

where A is the amplitude of the displacement-controlled excitation, m is the pendulum mass, and L is the pendulum effective length. Here, the pendulum effective length refers to the distance between the pendulum pivot point and the pendulum system center of mass, which consists of the pendulum shaft and sphere. Because the mass in any physical system is distributed along the pendulum shaft and bob, the effective length differs from the total length, l, and becomes an unknown parameter.

To develop the governing equation with Lagrange's method, it is necessary to obtain an expression for the potential energy when not in contact with the barrier

$$V = mgL(1 - \cos\theta). \tag{2}$$

Writing Lagrange's equation in terms of the generalized coordinate, θ, gives

$$\frac{d}{dt}\left(\frac{\partial T}{\partial\dot{\theta}}\right) - \frac{\partial T}{\partial\theta} + \frac{\partial V}{\partial\theta} = 0. \tag{3}$$

The resulting equation of motion that describes the pendulum oscillations during both contact and noncontact regimes is

$$\ddot{\theta} + 2\zeta\omega\dot{\theta} - \frac{A\Omega^2}{L}\ \sin\Omega t\ \cos\theta + \omega^2\ \sin\theta + H(\theta)\frac{lF_c(\theta)}{mL^2} = 0, \tag{4}$$

where $F_c(\theta)$ is the contact force that occurs at distance l from the pendulum pivot point, ζ is the damping ratio, $\omega = \sqrt{g/L}$ is the pendulum natural frequency, and $H(\theta)$ is the Heaviside step function that obeys

$$H(\theta) = \begin{cases} 1 & \text{for}\,\theta < 0 \\ 0 & \text{for}\,\theta \geq 0 \end{cases} \tag{5a}$$

3.1 Modeling the impact event

Various models can be implemented to investigate the dynamic behavior of an impact oscillator. In particular, a coefficient of restitution model can be implemented under the assumption of an instantaneous impact. While the simplest approach is to assume a constant coefficient of restitution, a more accurate approach requires experimentally determining a velocity-dependent coefficient of restitution. However, one should consider that this type of model neglects the finite time required for an impact to occur (see Fig. 3). An apparent disconnect also occurs when attempting to relate an empirically or experimentally determined coefficient of restitution to common material properties such as the elastic modulus and/or parameters describing the material's viscoelasticity.

This paper models the contact force expression based upon the work of Hunt and Crossley [10]. The resulting expression contains nonlinear elastic and

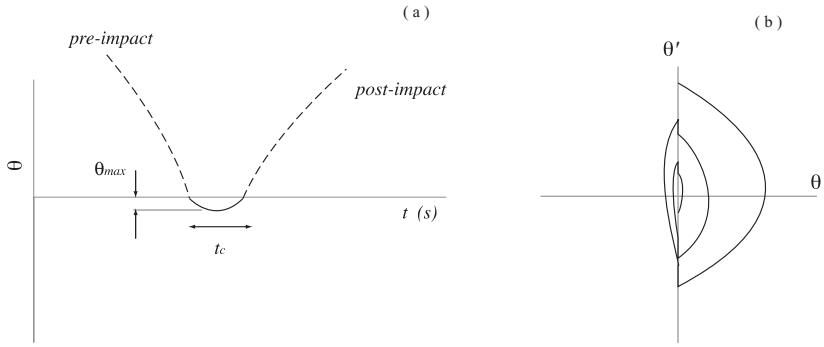

Fig. 3 Schematic diagram of a single impact event of duration t_c that reaches a maximum angle of $\theta_{\max}$ is shown in graph (a). Graph (b) provides a representative phase space diagram for the nonsmooth behavior of the unforced impact oscillations

viscoelastic forces,

$$F_c(\theta) = \frac{4E\sqrt{R}}{3}\left(1 + \mu_o l\dot{\theta}\right)(l\ \sin\theta)^{3/2}, \tag{6}$$

where E is the elastic modulus of the material barrier, μ_o is a material viscoelastic constant, and R is the spherical pendulum radius. This model incorporates Hertz's contact law for elastic conformal contact [12], while replicating the realistic force relationships at the beginning and end of of impact [10]. A primary assumption for this contact model is that the spherical pendulum can be treated as a rigid indenter. However, this assumption is justified since the modulus of the stainless steel sphere is orders of magnitude greater than the estimated modulus of the polytetrafluoroethelyne barrier.

4 Unforced oscillations

This section describes the work to identify the model parameters of the physical system that correspond to the governing equation of the previous section. The parameter identification process and unforced oscillation experiments are separated into two distinct steps: (1) the unforced experimental tests are performed with the impact barrier removed to identify parameters ζ, L, and ω from Equation (7); and (2) the unforced impact oscillations are compared with numerical simulation to obtain parameter estimates for E and μ_o of Equation (6). The equation for the unforced impact oscillator, which is given by

$$\ddot{\theta} + 2\zeta\omega\dot{\theta} + \omega^2\ \sin\theta + H(\theta)\frac{lF_c(\theta)}{mL^2} = 0, \tag{7}$$

will be further discussed throughout this section.

A summary of the expected behavior for the unforced oscillations of the impacting pendulum is shown Fig. 3. This schematic diagram illustrates that contact will occur over a finite duration time, t_c, and that the penetration depth, for a given set of colliding bodies, is dependent upon the preimpact states of the system. Additionally, this graph provides a phase space diagram of the unforced oscillations. In contrast to the smooth phase space of a continuous dynamical system, the vector field that describes a discontinuous dynamical system will be nonsmooth.

4.1 Unforced and nonimpacting oscillations

When the barrier is removed, the contact force of Equation (7) can be set to zero, $F_c(\theta) = 0$. Obtaining an approximate analytical solution to Equation (7) requires an expansion of the $\sin\theta$ term into a Taylor series about the downward position,

$$\omega^2\ \sin\theta \approx \omega^2\left(\theta - \frac{1}{6}\theta^3\right) = \omega^2\theta + \beta\theta^3, \tag{8}$$

where $\beta = -\omega^2/6$ and the terms of the order $\mathcal{O}\left(\theta^5\right)$ have been truncated from the expansion. After substituting Equation (8) into Equation (7), the approximate equation of motion can be written as

$$\ddot{\theta} + 2\zeta\omega\dot{\theta} + \omega^2\theta + \beta\theta^3 = 0. \tag{9}$$

The method of averaging is then applied by assuming a solution in the following solution form

$$\theta(t) = a\ \cos(\omega t + \phi) = a\ \cos\psi, \tag{10}$$

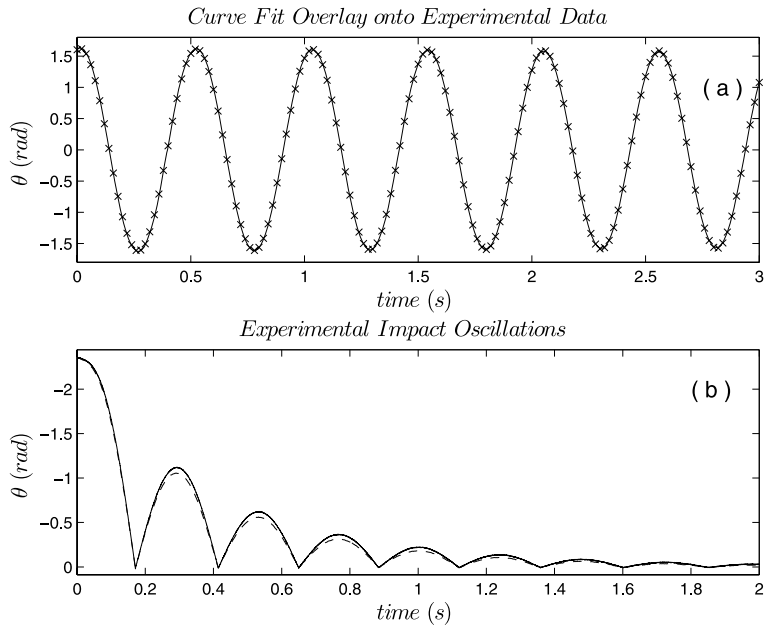

Fig. 4 Unforced oscillation time histories presented to illustrate: (a) the match between the approximate analytical solution (x) and the experimental data (*solid line*) for the unforced pendulum in the absence of a barrier; and (b) an example experimental impact oscillation data set (*solid line*) plotted against numerical data (*dashed line*)

where $\psi = \omega t + \phi$. Applying the averaging equations [15], will result in the following expressions for slow variations of a and ϕ,

$$\dot{a} = \frac{1}{2\pi\omega}\int_0^{2\pi} \sin\theta f\,(a\,\cos\psi, -a\omega\,\sin\psi)$$
$$d\theta = -\zeta\omega a, \tag{11a}$$
$$\dot{\phi} = \frac{1}{2\pi\omega a}\int_0^{2\pi} \cos\theta f\,(a\,\cos\psi, -a\omega\,\sin\psi)\,d\theta$$
$$= \frac{3a^2\beta}{8\omega}. \tag{11b}$$

The amplitude and phase relationships are obtained after solving for a and ϕ, respectively. Once $\beta = -\omega^2/6$ is substituted back into the integrated equations, the resulting relationships are

$$a = a_0 e^{-\zeta\omega t}, \tag{12a}$$
$$\phi = \frac{a_0^2}{32\zeta}\left(e^{-2\zeta\omega t} - 1\right) + \phi_0, \tag{12b}$$

where a_0 and ϕ_0 are constants of integration. If the system is started from rest with an initial angular displacement of ϑ_0, the resulting transient solution becomes

$$\theta(t) = \vartheta_0 e^{-\zeta\omega t}\,\cos\left(\omega t + \frac{\vartheta_0^2}{32\zeta}\left(e^{-2\zeta\omega t} - 1\right)\right), \tag{13}$$

which is in direct agreement with the multiple scales analysis of reference [16]. Ten independent free-fall oscillation tests were recorded for 10 s time intervals at a sample rate of 300 Hz. Using different start angles, the estimated parameters were averaged over the total number of records to minimize the influence of experimental noise. Figure 4 shows the result of one experimental test with an overlay of a nonlinear least squares solution, which illustrates the good agreement (see method in reference [17]). The estimated effective pendulum length was $L = 46 \pm .01$ mm and the estimated damping ratio was $\zeta = 0.007 \pm .0001$ with a 95% confidence level.

4.2 Unforced impact oscillations

This section describes the methods applied to estimate the elastic and viscoelastic parameters associated with the finite time impact model from experimental data. Thirty repeated experimental trials, see sample result in Fig. 4b, were performed during the course of this study. The procedure for each experimental trial required positioning the pendulum to the vertical location and allowing it to free-fall and repeatedly strike the barrier until the oscillations ceased. The motivation for the numerous trials came from the need to capture multiple realizations of the relatively short duration impact, where each trial was recorded at a different sample

rate. For instance, measurements at the lowest sample rate, 100 Hz, provided data with minimal measurement noise, but it was difficult to capture an adequate number of data samples during contact. At the highest sample rate, 200 kHz, a large number of contact samples were captured, but the measurement noise was prohibitively large. Therefore, only the experimental records sampled between 5–40 kHz were used for numerical comparison.

Numerical simulation of Equation (7) was combined with a nonlinear least-squares optimization to estimate the parameters for the finite time impact model. Two primary challenges for an effective numerical simulation are discontinuity detection and the ability to precisely determine the time step required to reach the surface of discontinuity. The numerical studies for this paper were performed using a fourth-order predictor-corrector Runge–Kutta algorithm along with the approach proposed by Henon [18]. In this method, the role of the independent variable (time) and dependent variable (displacement) are exchanged for a single integration step to determine the precise time step to reach the discontinuity point. This allows one to keep the numerical integration error within the tolerance of the Runge–Kutta procedure. As shown in Fig. 4, for the estimated parameters $E = 2$ MPa and $\mu_o = 0.75$ s/m, comparable results are obtained.

5 Forced oscillations

This section describes the experimental results for the forced oscillatory behavior of the impacting pendulum system and compares select results with numerical simulation. A nondimensionalized version of the governing equation, Equation (4), was used during numerical studies. This equation is obtained by introducing a nondimensional time, $\tau = \Omega t$,

$$\theta'' + 2\zeta\eta\theta' - \beta \sin\tau \cos\theta + \eta^2 \sin\theta + \gamma H(\theta)(1 + \mu\theta')\theta^{3/2} = 0, \tag{14}$$

where the following parameter substitutions have been implemented

$$\eta = \omega/\Omega, \tag{15a}$$

$$\beta = \frac{A}{L}, \tag{15b}$$

$$\gamma = \frac{4E\sqrt{R}}{3m\Omega^2 L^2} l^{5/2}, \tag{15c}$$

$$\mu = \mu_o l \Omega. \tag{15d}$$

5.1 Experimental investigation

Experimental tests were performed by either incrementally varying the shaker amplitude or the excitation frequency while recording time history data of the pendulum angular position, the shaker amplitude, and the laser tachometer timing pulse at a sample rate of 500 Hz. During the first series of experimental tests, the excitation frequency was set to 2 Hz and the shaker amplitude was incrementally varied. With regards to the nondimensionalized system presented in Equation (14), this corresponds to variations in β while holding the other parameters to the following constant values $\mu = 0.471$, $\eta = 1.162$, and $\gamma = 1.888 \times 10^4$. Figure 5 shows three example tests where periodic attractors were observed. Each row provides a 5 s snapshot of the 30 s recorded time history and a FFT (fast Fourier transform) diagram that elucidates the presence of multiple superharmonics. Apart from the data records shown, several other shaker amplitudes were surveyed and shown to still provide periodic data with several superharmonics.

A second series of experimental tests were performed by slowly varying the shaker amplitude while fixing the excitation frequency to a constant 10 Hz. The corresponding model parameters for Equation (14) are: $\mu = 2.356$, $\eta = 0.232$, and $\gamma = 755.5$. Figure 6 shows a snapshot of the time series alongside the frequency spectrum for each experimental trial. It is interesting to note that each of these examples, denoted by cases d–f, illustrate the presence of period-two and period-three subharmonics. In addition, the motion complexity was observed to increase for some shaker amplitudes due to the increased presence of incommensurate frequencies or quasi-periodic motions [20].

Figure 7 shows three examples where chaotic behavior was suspected during the experimental trials. In each example presented, the excitation frequency was set to 10 Hz and the angular oscillations were sampled at 500 Hz for a time interval of 360 s. A 15 s snapshot of the recorded time history is shown along with the corresponding Poincaré section in Fig. 7. Since only angular displacements were recorded, visualization of the qualitative features of each chaotic attractor required the

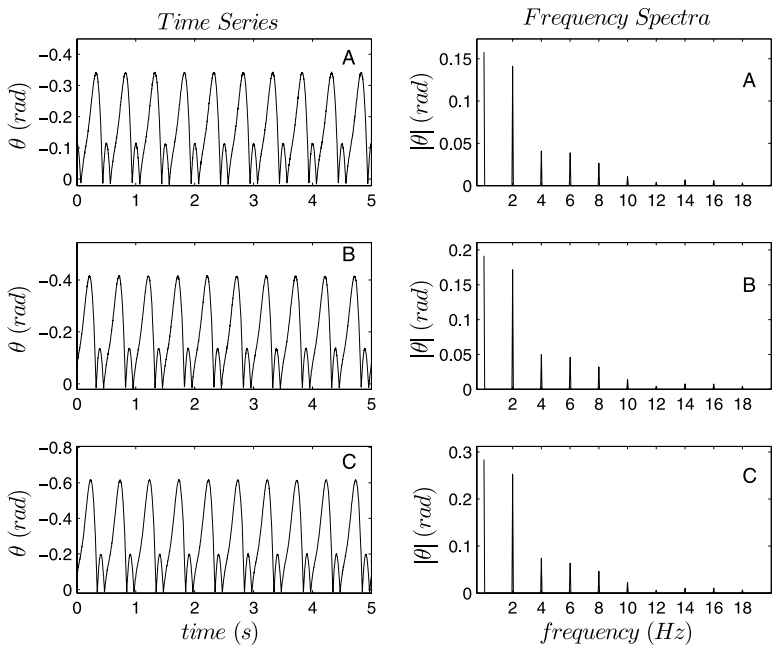

Fig. 5 Experimental time series and frequency spectra graphs recorded for the pendulum system at an excitation frequency of 2 Hz, $\eta = 1.162$. The excitation amplitudes for the above three cases defined by: (a) $\beta = 0.375$, (b) $\beta = 0.458$, (c) $\beta = 0.685$

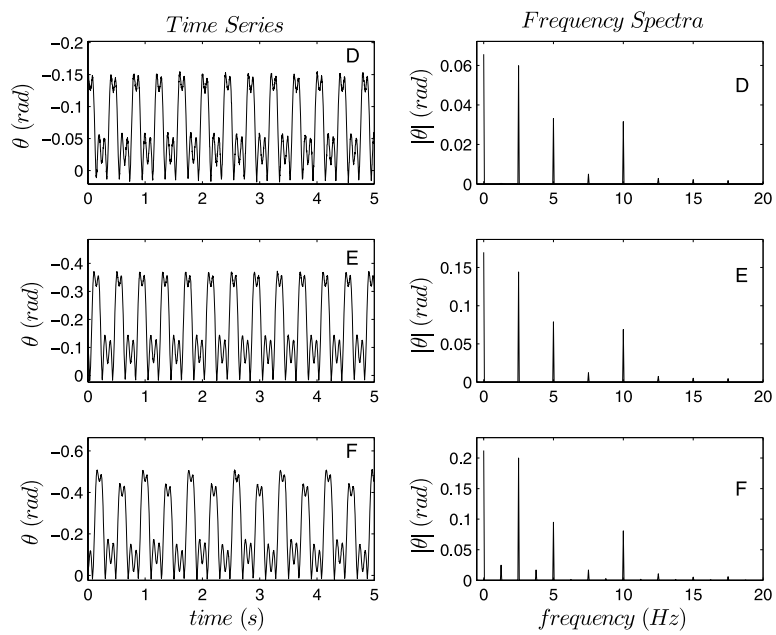

Fig. 6 Experimental time series and frequency spectra graphs recorded for the pendulum system at an excitation frequency of 10 Hz, $\eta = 0.232$. The excitation amplitudes for the above three cases defined by: (d) $\beta = 0.030$, (e) $\beta = 0.064$, (f) $\beta = 0.078$

application of delayed embedding techniques to reconstruct a topologically equivalent phase space in angular displacement $\theta(t_n)$ versus delayed angular displacement $\theta(t_n + \Delta t)$ coordinates. Following the methods suggested in [19], algorithms were developed to graph the mutual information function for the time series and the same time series shifted by Δt. The first minimum of the mutual information graph was used as the time shift or delay between the original time series and the $\theta(t + \Delta t)$ time series that are presented in Fig. 7.

5.2 Numerical comparisons

This section describes numerical investigations performed for comparative study with the observed experimental behavior. As discussed previously,

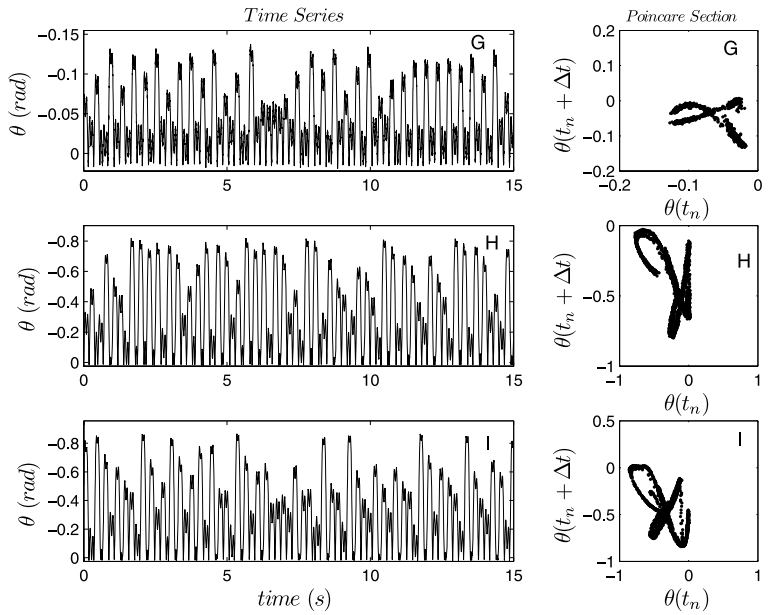

Fig. 7 Experimental time series and Poincaré sections for three experimental trials at an excitation frequency of 10 Hz, $\eta = 0.232$. The excitation amplitudes for the above three cases defined by: (G) $\beta = 0.022$, (H) $\beta = 0.114$, (I) $\beta = 0.120$

numerical algorithms used a fourth-order predictor-corrector Runge–Kutta approach along with the proposed method of Henon [18] for finding the surface of discontinuity. Figure 8 shows the first set of comparative examples. Numerical studies show comparable time series and frequency content as the results of cases (a) $\beta = 0.375$ and (c) $\beta = 0.685$ of Fig. 5 . However, the spectral amplitudes at each frequency do differ from those observed experimentally. The numerical study of case (d) $\beta = 0.030$ proved to have multiple periodic attractors with the closest comparable result shown in the bottom graphs of Fig. 8. When comparing these results to the experimental data of Fig. 6, both examples display period two behavior and contain strong subharmonic content. However, the experimental example is shown to contain an additional subharmonic of the order three.

In the final set of comparisons, the chaotic experimental examples are studied numerically. Figure 9 shows the results of the numerical studies carried out for the experimental trials of Fig. 7. The numerical result for case (g) $\beta = 0.022$ is shown to exhibit period-doubling behavior and differs from the chaotic behavior of the experimental system. Due to this apparent disagreement, a number of initial conditions were attempted. However, each numerical trial resulted in the same periodic attractor with subharmonic motion, but detailed basins of attraction were not constructed. The results of the final two cases, (h) $\beta = 0.114$ and (i) $\beta = 0.120$, are shown to qualitatively match the observed experimental chaotic behavior. In fact, a large number of initial conditions were investigated and found to yield chaotic behavior.

6 Summary and conclusions

This paper examines the dynamic behavior of a parametrically excited planar pendulum subjected to a motion-dependent discontinuity. Nonlinear force–deformation and force–velocity relationships previously suggested in the literature are investigated as a prescribed model for an impact event that is of finite time duration. This approach is in contrast to modeling the contact event with a coefficient of restitution or as a sharp impulse. While one may question the need for this additional modeling complexity, the observation of the authors was that a constant coefficient of restitution model provided a poor match between the experiment and numerical studies. One reason for this result is that a viscoelastic material was used for the impact barrier; this type of material has a velocity-dependent impact force and seems to significantly alter the contact time for low to intermediate impact velocities.

Since the dynamics of this system are piecewise smooth, the task of system identification was divided

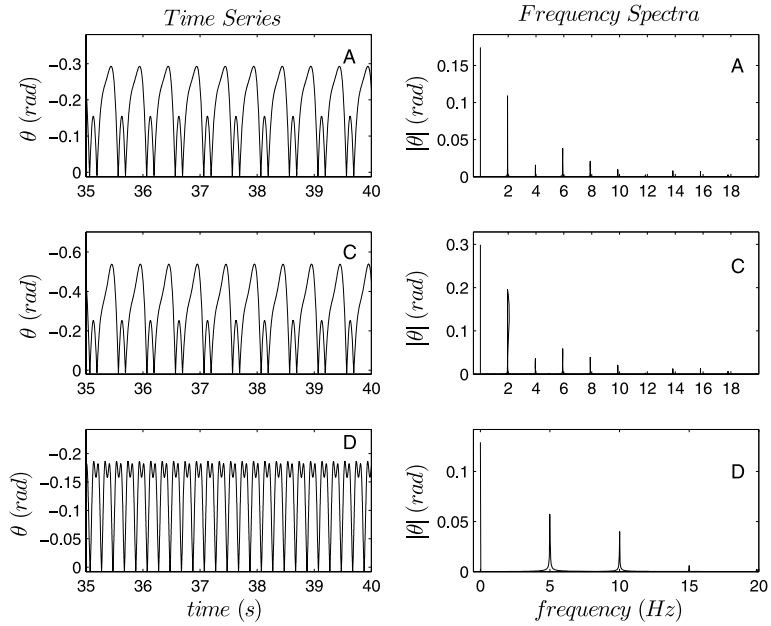

Fig. 8 Numerically generated time series and frequency spectra graphs for comparison with the experimental cases (a) $\beta = 0.375$ and (c) $\beta = 0.685$ of Fig. 5 and case (d) $\beta = 0.030$ of Fig. 6.

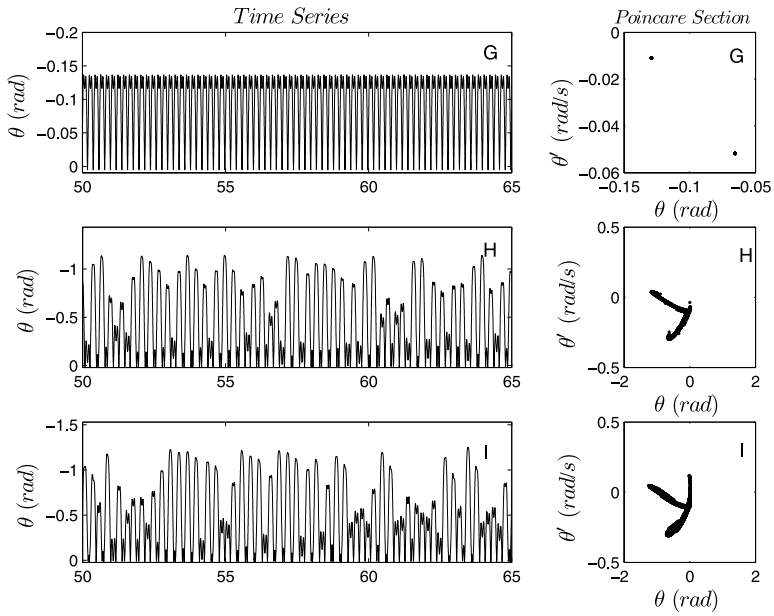

Fig. 9 Numerically generated time series and and Poincaré sections for comparison with the experimental cases (g) $\beta = 0.022$, (h) $\beta = 0.114$, and (i) $\beta = 0.120$ of Fig. 7.

into two separate tasks, which consisted of identifying the model parameters during contact and out of contact. More specifically, the results of an averaging solution are combined with a gradient-based optimization routine for the out-of-contact motions and the application of third-order smoothing splines, numerical simulation, and gradient-based optimization are used to identify model parameters during contact.

Experimental efforts include the fabrication of an experimental system and carrying out forced and unforced experimental trials. Numerical and experimental studies demonstrate the presence of multiple periodic attractors, chaotic oscillations, subharmonics, and quasi-periodic behavior. While not every experimental behavior is replicated with numerical study, reasonable agreement is found between the numerous

experimental and numerical cases studied when applying a finite time model for contact.

Acknowledgements Support from US National Science Foundation CAREER Award (CMS-0636641) is gratefully acknowledged.

References

1. Wiercigroch, M., Kraker, B.: Applied Nonlinear Dynamics and Chaos of Mechanical Systems with Discontinuities. Cambridge University Press, Cambridge, UK (2000)
2. Mann, B.P., Garg, N.K., Young, K.A., Helvey, A.M.: Milling bifurcations from structural asymmetry and nonlinear regeneration. Nonlinear Dyn. **42**, 319–337 (2005)
3. Nordmark, A.B.: Non-periodic motion caused by grazing incidence in an impact oscillator. J. Sound Vib. **145**(2), 279–287 (1991)
4. Moore, D.B., Shaw, S.W.: The experimental response of an impacting pendulum system. Int. J. Non-Linear Mech. **25**, 1–16 (1990)
5. Quinn, D.D.: Finite duration impacts with external forces. J. Appl. Mech. **72**, 778–784 (2005)
6. Bayly, P.V., Virgin, L.N.: An experimental study of an impacting pendulum. J. Sound Vib. **164**(2), 363–374 (1993)
7. Bayly, P.V.: On the spectral signature of weakly bilinear oscillators. J. Vib. Acoust. **118**, 353–361 (1996)
8. Shaw, S.W., Holmes, P.J.: A periodically forced piecewise linear oscillator. J. Sound Vib. **90**, 129–155 (1983)
9. Zeebroeck, M.V., Tijskens, E., Liedekerke, P.V., Deli, V., Baerdemaeker, J.D., Ramon, H.: Determination of the dynamical behavior of biological materials during impact using a pendulum device. J. Sound Vib. **266**, 465–480 (2003)
10. Hunt, K.H., Crossley, F.R.E.: Coefficient of restitution interpreted as damping in vibroimpact. J. Appl. Mech. **97**, 440–445 (1975)
11. Ladislav, P., Paterka, F.: Impact oscillator with Hertz's model of contact. Meccanica **38**, 99–114 (2003)
12. Johnson, K.L.: Contact Mechanics. Cambridge University Press, Cambridge, UK (1985)
13. Hertz, H.: On the elastic contact of solids. J. für die reine und Angewandte Mathematik **92**, 156–171 (1881)
14. Slade, K.N., Virgin, L.N., Bayly, P.V.: Extracting information from interimpact intervals in a mechanical oscillator. Phys. Rev. E **56**(3), 3705–3708 (1997)
15. Nayfeh, A.H., Mook, D.T.: Nonlinear Oscillations. Wiley, New York (1979)
16. Mann, B.P., Koplow, M.A.: Symmetry breaking bifurcations in a parametrically excited pendulum. Nonlinear Dyn. **46**(4), 427–437
17. Coleman, T., Li, Y.: An interior, trust region approach for nonlinear minimization subject to bounds. SIAM J. Optimization **6**, 418–445 (1996)
18. Henon, M.: On the numerical computation of Poincaré maps. Phys. D **5**, 412–414 (1982)
19. Kantz, H., Schreiber, T.: Nonlinear Time Series Analysis. Cambridge University Press, Cambridge, UK (2003)
20. Virgin, L.N.: Introduction to Experimental Nonlinear Dynamics, 2nd edn. Cambridge University Press, Cambridge, UK (2000)